Supporting Information

Arai et al. 10.1073/pnas.0908278107

SI Materials and Methods

Cell Preparations. *Dictyostelium discoideum* cells were used for all experiments. Halo-tag was fused with PTEN at the C terminus (PTEN-Halo). The function of the PTEN-Halo protein was confirmed by introducing an expression vector for PTEN-Halo into *pten*-null cells lacking the intrinsic PTEN protein (1). PTEN-Halo was visualized by vital staining with fluorescent Halo-ligands such as tetramethylrhodamine (TMR) in living cells. To observe the spatial and temporal dynamics of PTEN-Halo and $PH_{Akt/PKB}$-EGFP (or PI3K2-EGFP), both proteins were coexpressed in wild-type Ax-2 cells. To examine the contribution of PtdIns lipids metabolism enzymatic activities on the observed spatiotemporal dynamics, $PH_{Akt/PKB}$-EGFP and/or PTEN-Halo were expressed in *pi3k*-null (*pi3k1-5*$^{-}$, HM1200), *pten*-null, or *plc*-null cells. To visualize Ras activation, GFP-RBD, in which the Ras-binding domain of Raf1 is fused to GFP (2), was expressed in wild-type Ax-2 cells.

Cells were grown in HL-5 medium at 21 °C by a standard culture method (3). To obtain chemotactically competent cells, harvested cells were incubated at 2×10^6 cells/mL in development buffer (DB; 5 mM Na phosphate buffer, 2 mM $MgSO_4$, 200 μM $CaCl_2$, pH 6.5) for 5 h at 21 °C, leading to chemotactic competency with respect to cAMP. During the last 30 min of the incubation, caffeine, which inhibits adenylyl cyclase involved in the intrinsic cAMP production, was added to the extracellular fluid directly at a final concentration of 4 mM to reduce extracellular cAMP. To visualize PTEN-Halo in living cells, cells were treated with the fluorescent TMR-Halo-ligand (G8251; Promega) at 5–10 μM simultaneously with the caffeine treatment. After washing out the Halo-ligand, cells were incubated on a glass dish (3910-135; IWAKI) filled with DB supplemented with 4 mM caffeine for 5 min and then further incubated for at least 25 min in the presence or the absence of 5 μM latrunculin A (L5163; Sigma-Aldrich), an actin polymerization inhibitor, or LY294002, a PI3K inhibitor (4). Because caffeine treatment was required to observe any self-organized patterns, all experiments were performed in the presence of caffeine (*SI Discussion* and Fig. S1). To obtain vegetative cells, harvested cells were incubated in DB for 1 h (5).

For staining with phalloidin, an agar sheet was overlaid on the cells prepared as described above (6). After being allowed to settle for ~1 h, the cells were fixed in methanol containing 3.7% formaldehyde at −20 °C for 30 s and then in DB containing 3.7% formaldehyde at room temperature for 14 min and 30 s. Cells were washed twice in DB for 10 min, treated in blocking solution [1% BSA in 0.01% Tween-20 in PBS (TPBS)] for 30 min, and stained with Alexa488-phalloidin (A12379; Invitrogen) diluted at 1/50 by the blocking solution for 30 min. After being washed in TPBS twice for 10 min, cells were mounted in 50% glycerol in 2× PBS and observed under a confocal microscope.

Kymograph Analysis. Spatiotemporal dynamics of PTEN-TMR and $PH_{Akt/PKB}$-EGFP were analyzed from the time trajectoris of membrane localization. The fluorescence intensities of PTEN-TMR and $PH_{Akt/PKB}$-EGFP along the rounded cell contours were measured and plotted against an angle θ from an arbitrary position constant throughout the movie. The intensity line profile was obtained sequentially for each frame of the time-lapse movies. The resulting series of line profiles were plotted with time, showing the spatiotemporal dynamics of PTEN-TMR and $PH_{Akt/PKB}$-EGFP as a 2D pattern or so-called kymograph (Fig. 1*D*). Because the expression levels of both $PH_{Akt/PKB}$-EGFP and PTEN-TMR varied among individual cells even when a cloned cell line was used (Movie S3), cells expressing the proteins at an extremely low level were not further analyzed.

Auto- and Cross-Correlation Analysis. The temporal auto- and cross-correlation functions shown in Fig. 1 *F* and *G* were obtained from the fluorescence intensity data of PTEN-TMR and $PH_{Akt/PKB}$-EGFP shown in Fig. 1*D*. The temporal autocorrelation function is defined as $C(t) = \frac{\overline{(I(t)-\mu)\cdot(I(0)-\mu)}}{\sigma^2}$, where $I(t)$ is the fluorescence intensity of $PH_{Akt/PKB}$-EGFP or PTEN-TMR, and μ and σ are the mean and SD, respectively, of each. The line above the numerator indicates averaging. The temporal cross-correlation function is defined as $C_{PH\cdot PTEN}(t) = \frac{\overline{(I_{PH}(0)-\mu_{PH})\cdot(I_{PTEN}(t)-\mu_{PTEN})}}{\sqrt{\sigma_{PH}^2}\sqrt{\sigma_{PTEN}^2}}$, where $I_x(t)$ is the fluorescence intensity and μ_x and σ_x are the mean and SD of I_x, where x = PH or PTEN.

The spatiotemporal auto- and cross-correlation functions shown in Fig. 2 and Fig. S2 were obtained from kymographs. These functions clearly indicate spatiotemporal correlations in the localization of $PH_{Akt/PKB}$-EGFP and/or PTEN-TMR on the membrane when ordered patterns such as traveling waves or oscillations occur. Each kymograph corresponds to different single cells. The 2D autocorrelation functions for $PH_{Akt/PKB}$-EGFP and PTEN-TMR are defined as $C(\theta,t) = \frac{\overline{(I(\theta,t)-\mu)\cdot(I(0,0)-\mu)}}{\sigma^2}$, where $I(\theta, t)$ is the fluorescence intensity of $PH_{Akt/PKB}$-EGFP or PTEN-TMR at position θ along the membrane and at time t. μ and σ are the mean and SD of $I(\theta, t)$, respectively. Letting $I_{PH}(\theta, t)$ and $I_{PTEN}(\theta, t)$ be the fluorescence intensity data of $PH_{Akt/PKB}$-EGFP and PTEN-TMR, respectively, the spatiotemporal cross-correlation function is defined as $C_{PH\cdot PTEN}(\theta,t) = \frac{\overline{(I_{PH}(0,0)-\mu_{PH})\cdot(I_{PTEN}(\theta,t)-\mu_{PTEN})}}{\sqrt{\sigma_{PH}^2}\sqrt{\sigma_{PTEN}^2}}$.

Extracting the Averaged Temporal Evolution of PTEN and $PH_{Akt/PKB}$ Dynamics. The averaged temporal evolution shown in Fig. 4*A* was extracted from the time series of the PTEN-TMR and $PH_{Akt/PKB}$-EGFP fluorescence intensities along the cell membrane shown in Fig. 1*D* by using principal components analysis (PCA) as described below.

PCA was performed using $2n$ variables for the fluorescence intensities of PTEN-TMR and $PH_{Akt/PKB}$-EGFP, each with n time points at a given position. First, the PTEN-TMR and $PH_{Akt/PKB}$-EGFP fluorescence intensities were centered and normalized as follows. For $I_{PTEN}(\theta, t)$ and $I_{PH}(\theta, t)$, we constructed a vector, $\vec{U}(\theta,t)$, such that $U_j(\theta, t) = I_{PTEN}(\theta, t + (j - 1)\tau)$ and $U_{j+n}(\theta, t) = I_{PH}(\theta, t + (j - 1)\tau)$ with $j = 1, \ldots, n$. Here, $U_j(\theta, t)$ is the jth element of vector $\vec{U}(\theta,t)$, which consists of $2n$ elements. τ is the time interval of the time series. $\vec{U}(\theta,t)$was centered and normalized as $\vec{U}(\theta,t)$with $u_j(\theta,t) = \frac{U_j(\theta,t)-\mu_U}{\sigma_U}$, where μ_U and σ_U are the mean and SD of $\vec{U}(\theta,t)$(Fig. S3*A*).

Next, we performed PCA for $u(\theta,t)$ and obtained $2n$ principal components. Fig. S3*B* shows the percentage of total variance in the data explained by each principal component and the cumulative percentage for the first 10 principal components. A clear break exists between the second and third components, showing that the first 2 components are the most essential when describing the dynamics of PTEN and $PH_{Akt/PKB}$. The first two principal components, $\vec{v}^{(1)}$and $\vec{v}^{(2)}$, are shown in Fig. S3*C*. These two vectors can be considered a time series in which the jth and $(j + n)$th elements correspond to the values for PTEN and $PH_{Akt/PKB}$, respectively, at time $t = (j - 1)\tau$. Thus, in Fig. S3*C*, $\vec{v}^{(1)}$ and $\vec{v}^{(2)}$ are plotted as functions of time t. $\vec{v}^{(1)}$ and $\vec{v}^{(2)}$ are sinusoidal, providing clear evidence of the oscillatory

nature of the phosphatidylinositol reaction. From these two components, the period of oscillation was obtained (197 s). The phases of the two principal components differed by $\frac{\pi}{2}$ (Fig. S3*C*), indicating a reciprocal relation between PTEN and $PH_{Akt/PKB}$.

Whereas the first two components exhibited sinusoidal temporal evolutions, the overall temporal dynamics of PTEN and $PH_{Akt/PKB}$ concentrations were not expected to be sinusoidal. In other words, the principal components do not represent averaged dynamics. To obtain averaged dynamics, we next determined the oscillation phase for $\vec{u}(\theta,t)$ by using the first two principal components. The projection of $\vec{u}(\theta,t)$ onto the two components was obtained by calculating the inner product between $\vec{u}(\theta,t)$ and the principal components, giving $c^{(1)}(\theta,t)=\vec{u}(\theta,t)\cdot\vec{v}^{(1)}$ and $c^{(2)}(\theta,t)=\vec{u}(\theta,t)\cdot\vec{v}^{(2)}$. These two values define a point in space of the two principal components for $\vec{u}(\theta,t)$. Fig. S3*D* shows a scatter plot of $(c^{(1)}(\theta,t), c^{(2)}(\theta,t))$ for θ along the membrane at a given time *t*. $\phi(\theta,t)$ was obtained as an angular coordinate; i.e., $c^{(1)}(\theta,t)=r(\theta,t)\cos\phi(\theta,t)$ and $c^{(2)}(\theta,t)=r(\theta,t)\sin\phi(\theta,t)$. Fig. S3*D* indicates that $\phi(\theta,t)$ changes by 2π along the membrane.

To obtain the average time evolution, the time point of $I_{PTEN}(\theta,t)$ and $I_{PH}(\theta,t)$ was shifted by $-\phi(\theta,t)/\omega$ and averaged over an ensemble (Fig. S3*E*). Finally, we obtained the averaged time courses $\overline{I_{PTEN}(t)}$ and $\overline{I_{PH}(t)}$ of PTEN and $PH_{Akt/PKB}$, respectively, given by $\overline{I_{PTEN}(t)}=\langle I_{PTEN}(\theta,t_0+t-\frac{\varphi(\theta,t_0)}{\omega})\rangle_{\theta,t_0}$, and $\overline{I_{PH}(t)}=\langle I_{PH}(\theta,t_0+t-\frac{\varphi(\theta,t_0)}{\omega})\rangle_{\theta,t_0}$,

where $\langle\cdot\rangle_{\theta,t_0}$ indicates the average taken for θ and t_0. The averaged temporal evolution of PTEN and $PH_{Akt/PKB}$ dynamics was obtained by plotting $\overline{I_{PTEN}(t)}$ with $\overline{I_{PH}(t)}$ as shown in Fig. 4*A*. We applied this analysis to individual cells (Fig. S4), indicating that the characteristic crescent-shaped dynamics were commonly observed in cells even when they exhibited different modes of ordered patterns (Fig. 2).

Cell Migration Analysis. Cells were observed with an Olympus IX-71 inverted microscope equipped with phase contrast optics. Cell behavior was recorded with a cooled CCD camera (MicroMax; Princeton Instruments) and MetaMorph software (Molecular Devices) in a personal computer. Cell images were acquired at 5-s intervals for 20 min. To analyze the motile activities of the cells, cell images were processed automatically by using laboratory-developed software. From the positional changes, migration velocity was calculated (7).

SI Discussion

Caffeine Treatment. Self-organization of the PtdIns lipids system was observed in the presence of caffeine. After washing out the caffeine, the number of cells with $PH_{Akt/PKB}$-EGFP-enriched domains dramatically decreased (Fig. S1), which is consistent with a previous report (8). However, we should note that transient generations of membrane-bound $PH_{Akt/PKB}$-EGFP-enriched domains were often observed even without caffeine, although the domains disappeared immediately after their formation. Thus, caffeine has not only an inhibitory effect on cAMP production (4) but also a stabilizing effect on the self-organized pattern formation of the PtdIns lipid system, which enables us to observe chemoattractant-independent dynamics in the PtdIns lipids system. Because caffeine was applied uniformly with respect to space and time, caffeine itself is not a factor for externally breaking the spatiotemporal symmetry in the PtdIns lipids system.

Theoretical Model. To account for the generation of traveling waves by the PtdIns lipids system, we constructed a simple mathematical model. As shown in Fig. 3, the self-organized traveling waves of $PH_{Akt/PKB}$ and PTEN arise from membrane-bound PTEN and PI3K. These are necessary for self-organized traveling waves because the inhibition of PTEN and PI3K disrupted the self-organized pattern formation. PTEN acts as a phosphatase for PtdIns(3,4,5)P_3 to produce PtdIns(4,5)P_2, whereas PI3K acts as a kinase for PtdIns(4,5)P_2 to produce PtdIns(3,4,5)P_3 (9, 10). Thus, the concentrations of membrane-bound PtdIns(3,4,5)P_3 and PtdIns(4,5)P_2 are regulated by these enzymes. In addition, PtdIns(3,4,5)P_3 can be degraded in a PTEN-independent manner. This is because the *pten*-null cells lacking the PTEN gene exhibit at least partial degradation of PtdIns(3,4,5)P_3 (11). Additionally, PtdIns(4,5)P_2 can be supplied by PTEN-independent pathways (11–13) and degraded by PI3K-independent pathways (14). On the basis of the experimental observations, the concentration of PTEN was dependent on time and space. The concentration of PI3K was assumed to be uniform along the membrane (2). Therefore, in our theoretical model, the local state of the membrane is described by [PIP3], [PIP2], and [PTEN]. We also assumed that the fluorescence intensities of membrane-bound $PH_{Akt/PKB}$ are linearly proportional to the concentration of membrane-bound PtdIns(3,4,5)P_3.

We considered the local reaction dynamics to be oscillatory. In such cases, the period of oscillation is expected to be determined by reactions involving PTEN and PI3K, but independent of cell size, which is consistent with our finding that there was no correlation between the periods of oscillation and cell size (Fig. S4*N*). As shown in Fig. 4, the oscillation shows characteristics of a relaxation oscillator, in which two relatively stable states can be found: [PIP3] is low and [PTEN] is high or [PTEN] is low and [PIP3] is high. These states are connected by rapid transitions between them. Any model must explain these relaxation oscillator characteristics. We also considered the reciprocal relation between PTEN and $PH_{Akt/PKB}$, where the upper and lower branches can be well fitted by hyperbolic functions (Fig. 4*A*). To satisfy these constraints, we introduced PtdIns(3,4,5)P3-dependent negative regulation on PTEN recruitment to the membrane in which the association of PTEN to the membrane is suppressed by PtdIns(3,4,5)P_3 or the dissociation of PTEN from the membrane is enhanced by PtdIns(3,4,5)P_3 (Fig. 5*A*). This regulation operates as a positive feedback loop because increases and decreases in [PIP3] can respectively lead to further increases and decreases in [PIP3] by suppressing and enhancing PTEN membrane localization. When [PIP3] increases, [PTEN] decreases, thereby further increasing [PIP3], leading to the state with low [PTEN] and high [PIP3]. In contrast, the increase in [PTEN] accelerates the decrease in [PIP3], resulting in the state with low [PIP3] and high [PTEN]. Thus, the two states can be viewed as a consequence of positive feedback. Because [PIP3] is always much less than [PIP2] (11), we surmised that the two stable states can be attained without considerable depletion of PtdIns(4,5)P_2.

On the basis of these observations, we developed evolution equations for [PIP3], [PIP2], and [PTEN] given by

$$\frac{\partial[\mathrm{PIP3}]}{\partial t}=-R_{\mathrm{PTEN}}+R_{\mathrm{PI3K}}-\lambda_{\mathrm{PIP3}}[\mathrm{PIP3}]+D\nabla^2[\mathrm{PIP3}], \quad \textbf{[S1]}$$

$$\frac{\partial[\mathrm{PIP2}]}{\partial t}=R_{\mathrm{PTEN}}-R_{\mathrm{PI3K}}+k-\lambda_{\mathrm{PIP2}}[\mathrm{PIP2}]+D\nabla^2[\mathrm{PIP2}], \quad \textbf{[S2]}$$

$$\frac{\partial[\mathrm{PTEN}]}{\partial t}=V_{ass}[\mathrm{PTEN}]_{\mathrm{cyt}}\frac{[\mathrm{PIP2}]}{K_{\mathrm{PIP2}}+[\mathrm{PIP2}]}\frac{K_\alpha+\alpha[\mathrm{PIP3}]}{K_\alpha+[\mathrm{PIP3}]}-\lambda_{\mathrm{PTEN}}[\mathrm{PTEN}], \quad \textbf{[S3]}$$

with the catalytic reactions of PTEN and PI3K, R_{PTEN} and R_{PI3K}, given by

$$R_{\mathrm{PTEN}} = V_{\mathrm{PTEN}}[\mathrm{PTEN}]\frac{[\mathrm{PIP3}]}{K_{\mathrm{PTEN}}+[\mathrm{PIP3}]}, \quad \textbf{[S4]}$$

$$R_{\mathrm{PI3K}} = V_{\mathrm{PI3K}}\frac{\beta K_\beta + [\mathrm{PIP3}]}{K_\beta + [\mathrm{PIP3}]}\frac{[\mathrm{PIP2}]}{K_{\mathrm{PI3K}}+[\mathrm{PIP2}]}. \quad \textbf{[S5]}$$

In Eq. **S1**, the third term describes the PTEN-independent degradation of PtdIns(3,4,5)P_3. In Eq. **S2**, the third term gives the PTEN-independent supply of PtdIns(4,5)P_2, whereas the fourth term expresses PI3K-independent degradation of PtdIns(4,5)P_2. For the catalytic reaction of PI3K, R_{PI3K}, in Eq. **S5**, $(\beta K_\beta + [\mathrm{PIP3}])/(K_\beta + [\mathrm{PIP3}])$ was introduced to examine the positive regulatory effect of [PIP3] on the activity of PI3K ($0 \leq \beta \leq 1$) (15). The positive regulatory effect of [PIP3] on the activity of PI3K can be examined by changing β. When $\beta = 1$, $(\beta K_\beta + [\mathrm{PIP3}])/(K_\beta + [\mathrm{PIP3}])$ becomes 1, meaning that PI3K activity is not coupled to PIP3 distribution and thus PI3K activity is uniformly distributed along the membrane. When $\beta < 1$, PI3K activity is coupled to PIP3 distribution. With decreasing β values, the PI3K activity is localized more efficiently to PIP3-enriched regions. In Eq. **S3**, the first and second terms describe the association and dissociation of PTEN to and from the membrane, respectively. In the first term, $(K_\alpha + \alpha[\mathrm{PIP3}])/(K_\alpha + [\mathrm{PIP3}])$ represents the negative regulatory effects of [PIP3] on PTEN binding ($0 \leq \alpha \leq 1$). The PTEN association rate is dependent on the concentration of cytosolic PTEN, $[\mathrm{PTEN}]_{\mathrm{cyt}}$. We also studied the case when [PIP3] enhances the dissociation of PTEN from the membrane without any effect on its association, finding essentially the same results. Because the diffusion coefficient in the cytosol is much larger than that on the membrane (16), we assumed that the cytosolic PTEN concentration is uniform inside the cytosol. Thus, the cytosolic PTEN concentration, $[\mathrm{PTEN}]_{\mathrm{cyt}}$, is given by

$$[\mathrm{PTEN}]_{\mathrm{cyt}} = [\mathrm{PTEN}]_{total} - \chi\overline{[\mathrm{PTEN}]}, \quad \textbf{[S6]}$$

where $\overline{[\mathrm{PTEN}]}$ indicates the average concentration of membrane-bound PTEN and χ is a constant that transforms the membrane concentration to the cytosolic concentration. PtdIns(4,5)P_2 has been suggested as a putative binding site for PTEN (17). Thus, the effects of changes in PtdIns(4,5)P_2 concentration on PTEN membrane binding were described as $[\mathrm{PIP2}]/(K_{\mathrm{PIP2}}+[\mathrm{PIP2}])$ in the first term of Eq. **S3**. The diffusion of PtdIns lipids is described by the last terms in Eqs. **S1** and **S2** with the diffusion coefficient D. Because the diffusion length of PTEN before membrane dissociation is ~300 nm, within which time the PTEN concentration is expected to be uniform, we can safely ignore the diffusion effect of membrane-bound PTEN (18, 19).

For numerical simulations, we studied a one-dimensional system along the membrane. The radius of the cells, R, was chosen to be 5 μm, which is typical for latrunculin A-treated cells. The lattice was assigned to a 0.02-μm grid. The time step was 0.005 s. Parameters are summarized in Table S1. For the stochastic simulation, we used the τ-leap method (20).

First we consider the situation where the diffusion term is neglected and $[\mathrm{PTEN}]_{\mathrm{cyt}}$ is constant in time. Our model successfully produces the local reaction dynamics observed experimentally, including the clockwise oscillation following the characteristic crescent-shaped trace along the [PIP3]–[PTEN] coordinates. The major reactions generated by PTEN and PI3K described by the crescent-shaped dynamics are as follows. Local regions on the membrane usually adopt to the state with low [PIP3] and high [PTEN]. In this state, [PIP2] gradually increases due to both PTEN-dependent and PTEN-independent factors, causing PtdIns(4,5)P_2 to accumulate, and in turn drives PI3K-dependent PtdIns(3,4,5)P_3 production. The [PIP3] gradually increases due to the PI3K activation to eventually exceed a threshold, which inhibits PTEN membrane recruitment. This inhibition leads to a decrease in [PTEN] and further increase in [PIP3], sustaining the feedback loop. With the rapid increase in [PIP3], membrane-bound PTEN is depleted, leading to the state with high [PIP3] and low [PTEN]. In this state, [PIP2] is reduced because PTEN-dependent dephosphorylation of PtdIns(3,4,5)P_3 is reduced. Such a decrease in [PIP2] has a suppressive effect on PtdIns(3,4,5)P_3 production, causing a decrease in [PIP3] in combination with PTEN-independent PtdIns(3,4,5)P_3 degradation. This decrease in [PIP3] causes an increase in PTEN membrane recruitment by negative regulation, causing a further decrease in [PIP3] and an increase in [PTEN]. This positive feedback results in the state with low [PIP3] and high [PTEN], which is the original state of the oscillation.

Next, we consider the effects of globally integrating the local regions. Whereas the diffusion of membrane-bound PtdIns lipids introduces a local interaction of reaction dynamics, the fast diffusion of cytosolic PTEN results in globally integrating the PtdIns lipids reactions of these local regions while keeping the total PTEN concentration conserved. This global integration has a tendency to keep the total PTEN membrane concentration constant. Thus, the formation of a PTEN-enriched domain at a particular part of the membrane prevents the formation of domains at other parts. Furthermore, the fast PTEN cytosolic diffusion explains one element of the polarization generation mechanism. Incorporating global integration and local oscillatory dynamics, the spatiotemporal dynamics of the model generate a traveling wave as one possible outcome. The local oscillatory dynamics at individual regions along the membrane can be coordinated with each other through cytosolic PTEN, generating an asymmetric distribution of both PtdIns(3,4,5)P3 and PTEN in the whole cell.

We study the case when there is no positive regulatory effect of [PIP3] on PI3K ($\beta = 1$). Our deterministic and stochastic simulations successfully reproduce the traveling domain with an anticorrelative spatial profile between the PtdIns(3,4,5)P3 and PTEN concentrations (Fig. 5). Therefore, in addition to the enzymatic activities of PTEN and PI3K, the PtdIns(3,4,5)P_3-dependent negative regulation on PTEN recruitment plays an essential role for generating self-organized patterns within the PtdIns lipids system. Overall, our model is able to reproduce the self-organized patterns including traveling waves, spatiotemporal oscillation, and stationary domains by changing various parameters such as PTEN and PI3K concentrations.

The two types of RBD dynamics observed in living cells can also be explained, in this case by varying parameter β in Eq. **S5**. By decreasing β, the positive regulatory effect of [PIP3] on PI3K activity becomes stronger, meaning PI3K activity is coupled to PIP3 distribution along the membrane. Although the positive regulatory effect of [PIP3] on PI3K is not essential for the PtdIns(3,4,5)P_3/PTEN wave generation in our model, positive regulation is seen to stabilize the PtdIns(3,4,5)P_3-enriched state when [PIP3] is high, whereas the PTEN-enriched state is stable when [PIP3] is low. As a result, the positive feedback from [PIP3] to PI3K appears to have a role in stabilizing the self-organized traveling waves of the phosphatidylinositol lipids signaling system.

Negative Regulation of PTEN Localization by PtdIns(3,4,5)P_3. We observed PTEN-TMR localization in both wild-type and *pi3k1-5*-null cells treated with latrunculin A and analyzed the kymographs of PTEN localization by calculating the spatiotemporal autocorrelation function (*SI Materials and Methods*). Most wild-type cells showed PTEN localization moving along the entire membrane for >30 min (Fig. S2 *A* and *B*) ($n = 32$). In 72% of wild-type cells, high spatiotemporal correlation was detected in the spatiotemporal autocorrelation analysis, which exhibited either traveling waves (Fig. S2 *A* and *B*) or oscillations. On the

other hand, in the *pi3k1-5*-null cells, only one cell showed traveling waves that did not last for >10 min. In the others (n = 59), PTEN localization was either transient or spatiotemporally static with slight fluctuations in the location (Fig. S2 *C* and *D*). In *pi3k1-5*-null cells, a similar spatiotemporal correlation was negligible except for the case of one showing transient traveling waves. From these results, we conclude that PI3K is required for continuous traveling waves or spatiotemporal oscillations of PTEN localization. In *pi3k1-5*-null cells, almost no PtdIns(3,4,5)P_3 was detectable on the membrane, which is due to the overwhelming activity of PTEN. In *pten*-null cells, the PtdIns(3,4,5)P_3 was uniformly localized on the membrane and the PtdIns(3,4,5)P_3 wave was not observed (Fig. 3*A*). Thus, the PtdIns(3,4,5)P_3/PTEN wave requires both PI3K-dependent production and PTEN-dependent degradation of PtdIns(3,4,5)P_3.

We next observed PTEN-TMR localization in locomoting cells. In wild-type cells, PTEN showed membrane localization at lateral and posterior regions, but not the leading edge of pseudopods (Fig. 6*A*). F-actin staining with phalloidin showed a clear and dense accumulation of F-actin at the leading edge, whereas PTEN localization was anticorrelative with F-actin accumulation beneath the membrane (Fig. 6*B*). In *pi3k1-5*-null cells, an almost homogenous PTEN localization was observed along the entire membrane, including the leading edges (Fig. 6*A*). At the leading edge, F-actin accumulated beneath the membrane where PTEN showed localization (Fig. 6*B*). Our results show that PTEN is mislocalized at the pseudopods in the absence of PtdIns(3,4,5)P_3, suggesting that PTEN localization is at least in part under the regulation of PtdIns(3,4,5)P_3. On the basis of these observations, we hypothesize negative regulation of PTEN localization by PtdIns(3,4,5)P_3.

As shown previously, PTEN is absent in regions on the membrane facing higher cAMP concentrations in the absence of PtdIns(3,4,5)P_3, indicating the existence of a PtdIns(3,4,5)P_3-independent mechanism for PTEN localization in the presence of cAMP (21). On the other hand, we showed that PTEN localization is somehow regulated in a PtdIns(3,4,5)P_3-dependent manner in the absence of cAMP. These observations suggest at least two mechanisms for PTEN localization: one PtdIns(3,4,5)P_3 dependent and the other PtdIns(3,4,5)P_3 independent. The former mechanism is involved in PtdIns(3,4,5)P_3/PTEN wave generation related to random cell migration in the absence of a cAMP gradient; the latter has an indispensable role in polarized PTEN localization in response to a cAMP gradient.

1. Matsuoka S, Miyanaga Y, Yanagida T, Ueda M (2008) In *Single-Molecule Techniques*, eds Selvin PR, Ha T (Cold Spring Harbor Lab Press, Cold Spring Harbor, NY), pp 239–258.
2. Sasaki AT, Chun C, Takeda K, Firtel RA (2004) Localized Ras signaling at the leading edge regulates PI3K, cell polarity, and directional cell movement. *J Cell Biol* 167: 505–518.
3. Watts DJ, Ashworth JM (1970) Growth of myxameobae of the cellular slime mould Dictyostelium discoideum in axenic culture. *Biochem J* 119:171–174.
4. Brenner M, Thoms SD (1984) Caffeine blocks activation of cyclic AMP synthesis in Dictyostelium discoideum. *Dev Biol* 101:136–146.
5. Sasaki AT, et al. (2007) G protein-independent Ras/PI3K/F-actin circuit regulates basic cell motility. *J Cell Biol* 178:185–191.
6. Fukui Y, Yumura S, Yumura TK (1987) Agar-overlay immunofluorescence: High-resolution studies of cytoskeletal components and their changes during chemotaxis. *Methods Cell Biol* 28:347–356.
7. Sato MJ, et al. (2007) Input-output relationship in galvanotactic response of Dictyostelium cells. *Biosystems* 88:261–272.
8. Postma M, et al. (2004) Sensitization of Dictyostelium chemotaxis by phosphoinositide-3-kinase-mediated self-organizing signalling patches. *J Cell Sci* 117:2925–2935.
9. Van Haastert PJ, Devreotes PN (2004) Chemotaxis: Signalling the way forward. *Nat Rev Mol Cell Biol* 5:626–634.
10. Kölsch V, Charest PG, Firtel RA (2008) The regulation of cell motility and chemotaxis by phospholipid signaling. *J Cell Sci* 121:551–559.
11. Huang YE, et al. (2003) Receptor-mediated regulation of PI3Ks confines PI(3,4,5)P3 to the leading edge of chemotaxing cells. *Mol Biol Cell* 14:1913–1922.
12. Funamoto S, Meili R, Lee S, Parry L, Firtel RA (2002) Spatial and temporal regulation of 3-phosphoinositides by PI 3-kinase and PTEN mediates chemotaxis. *Cell* 109:611–623.
13. Iijima M, Devreotes P (2002) Tumor suppressor PTEN mediates sensing of chemoattractant gradients. *Cell* 109:599–610.
14. Kortholt A, King JS, Keizer-Gunnink I, Harwood AJ, Van Haastert PJ (2007) Phospholipase C regulation of phosphatidylinositol 3,4,5-trisphosphate-mediated chemotaxis. *Mol Biol Cell* 18:4772–4779.
15. Janetopoulos C, Firtel RA (2008) Directional sensing during chemotaxis. *FEBS Lett* 582: 2075–2085.
16. Postma M, Bosgraaf L, Loovers HM, Van Haastert PJ (2004) Chemotaxis: Signalling modules join hands at front and tail. *EMBO Rep* 5:35–40.
17. Iijima M, Huang YE, Luo HR, Vazquez F, Devreotes PN (2004) Novel mechanism of PTEN regulation by its phosphatidylinositol 4,5-bisphosphate binding motif is critical for chemotaxis. *J Biol Chem* 279:16606–16613.
18. Levine H, Kessler DA, Rappel WJ (2006) Directional sensing in eukaryotic chemotaxis: A balanced inactivation model. *Proc Natl Acad Sci USA* 103:9761–9766.
19. Gamba A, et al. (2005) Diffusion-limited phase separation in eukaryotic chemotaxis. *Proc Natl Acad Sci USA* 102:16927–16932.
20. Gillespie DT (2001) Approximate accelerated stochastic simulation of chemically reacting systems. *J Chem Phys* 115:1716–1733.
21. Hoeller O, Kay RR (2007) Chemotaxis in the absence of PIP3 gradients. *Curr Biol* 17: 813–817.

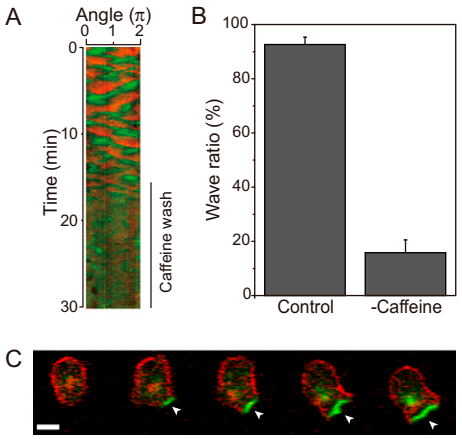

Fig. S1. Effects of caffeine treatment. *Dictyostelium* cells were placed on a flow chamber and pretreated with caffeine. (*A*) The kymograph shows that $PH_{Akt/PKB}$-EGFP- and PTEN-TMR-enriched regions disappeared after continuous buffer flow in the absence of caffeine (indicated as caffeine wash). (*B*) Inhibition of the self-organized wave in the absence of caffeine. Shown are wild-type (Control) cells in the presence of caffeine (95 cells, $n = 16$) and in the absence of caffeine (44 cells, $n = 6$). Caffeine was used at 4 mM. Data are mean ± SEM; *n*, number of independent experiments. (*C*) Time-lapse images of *Dictyostelium* cells coexpressing PTEN-TMR (red) and $PH_{Akt/PKB}$ -EGFP (green) in the vegetative stage. Arrowheads indicate a $PH_{Akt/PKB}$- enriched domain on the membrane. Time interval, 2 s. (Scale bar, 5 μm.)

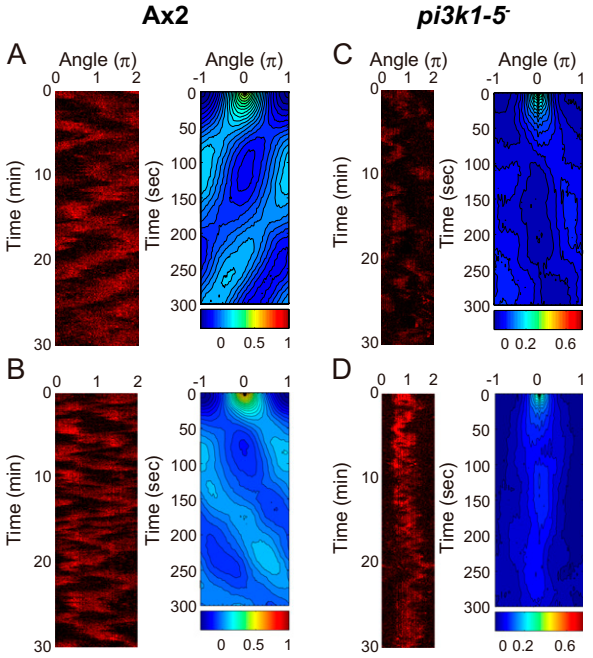

Fig. S2. PTEN localization without ordered patterns in *pi3k1-5*-null cells. (*A–D Left*) Kymographs of PTEN-TMR observed in individual wild type (*A* and *B*) and *pi3k1-5*-null (*C* and *D*) cells in the presence of 5 μM latrunculin A. (*A–D Right*) The corresponding spatiotemporal autocorrelation function of PTEN-TMR. Most wild-type cells showed ordered patterns, whereas only one *pi3k1-5*-null cell of 60 showed a transient traveling wave and the rest showed no ordered patterns. Results were confirmed by spatiotemporal autocorrelation analysis of PTEN-TMR.

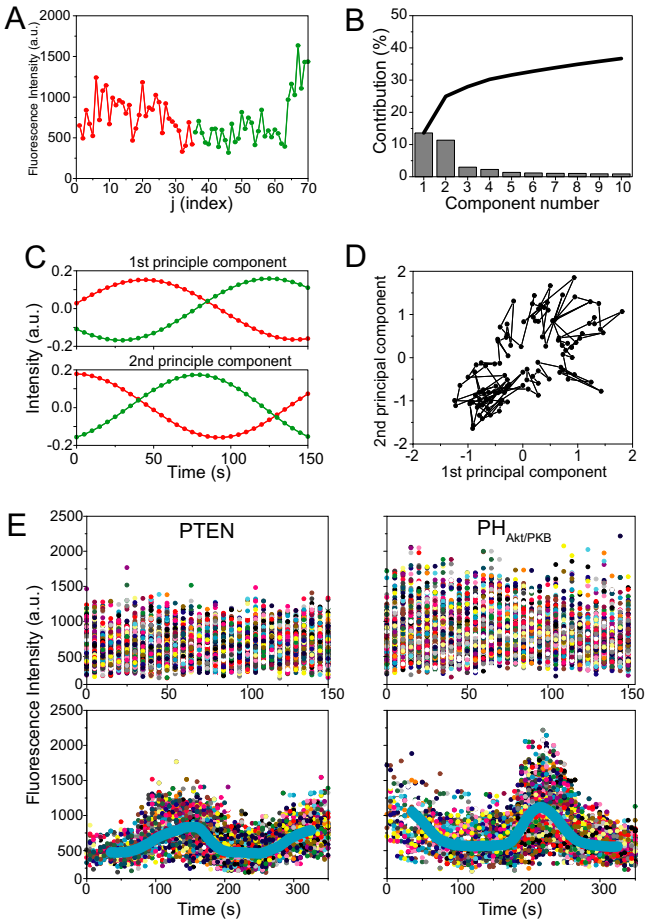

Fig. S3. Extracting the averaged temporal evolution of PTEN and $PH_{Akt/PKB}$ dynamics. (*A*) Vectorization of stochastic time series of fluorescence intensities of PTEN-TMR (red) and $PH_{Akt/PKB}$-EGFP (green). (*B*) The fraction of total variance in the data explained by each principal component and the cumulative percentage showed a clear break between the second and third components. (*C*) The first and second principal components plotted as a time series of PTEN and $PH_{Akt/PKB}$. (*D*) The projection of time series data onto the first two principal components. (*E*) Before (*Upper*) and after (*Lower*) aligned time series of fluorescence intensities of PTEN and $PH_{Akt/PKB}$ with phase differences (colors indicate individual time series) and averaged time evolution (solid lines).

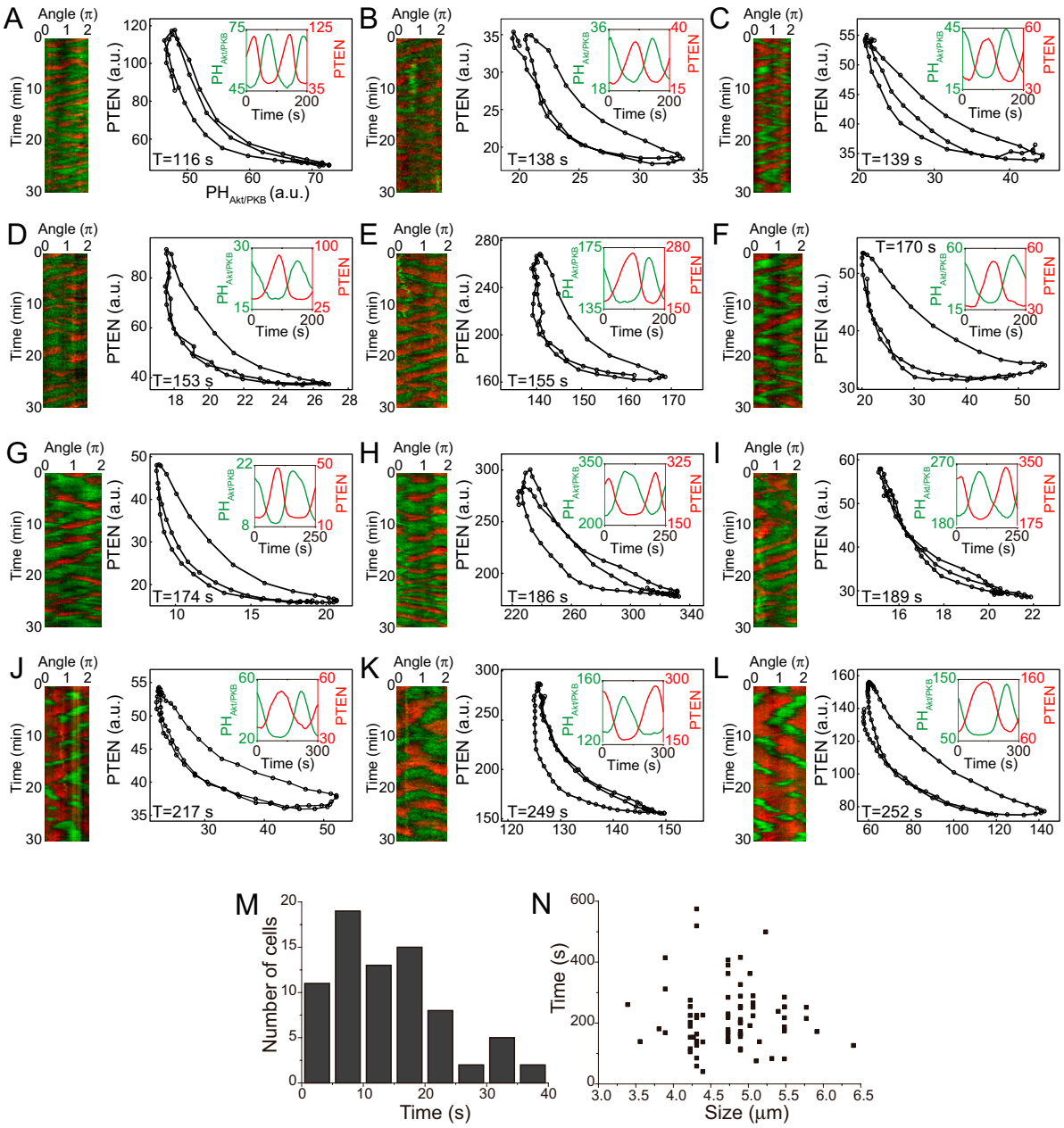

Fig. S4. Gallery of crescent-shaped dynamics. (*A–L*) Kymograph of PTEN-TMR (red) and $PH_{Akt/PKB}$-EGFP (green) in single cells showing different patterns and the corresponding averaged temporal evolution. The temporal evolutions were plotted at 5-s intervals. *T*, oscillation period (seconds). (*Insets*) Time trajectories of the averaged dynamics of PTEN-TMR (red) and $PH_{Akt/PKB}$-EGFP (green). (*M*) Histogram of the time delay obtained by a temporal cross-correlation function of the traveling waves. The mean ± SD value is 14.44 ± 9.19 s (n = 75 cells). (*N*) Scattered plot of cell radius and oscillation periods. No correlation between cell sizes and oscillation periods is seen. Each dot corresponds to individual cells.

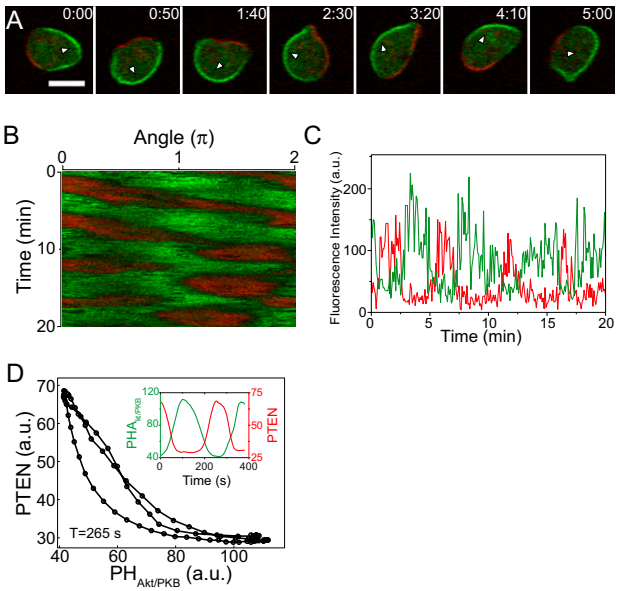

Fig. S5. Self-organized traveling waves of $PH_{Akt/PKB}$ and PTEN in cells treated modestly with latrunculin A. Cells were observed in the presence of 1–2.5 μM latrunculin A. In this condition, the cells can exhibit shape changes without efficient migration, which is due to partial inhibition of actin polymerization. (*A*) Time-lapse images of cells expressing PTEN-TMR (red) and $PH_{Akt/PKB}$-EGFP (green). Arrowheads indicate $PH_{Akt/PKB}$-enriched domains on the membrane. Time, min:s. (Scale bar, 10 μm.) Also see Movie S4. (*B*) Kymograph showing oscillatory patterns of PTEN-TMR (red) and $PH_{Akt/PKB}$-EGFP (green). (*C*) Time trajectories of fluorescence intensities for both PTEN-TMR and $PH_{Akt/PKB}$-EGFP on a subdomain of the membrane show the reciprocal relation. (*D*) The temporal evolutions are plotted at 5-s intervals and exhibit a characteristic crescent-shaped dynamics. *T*, oscillation period (seconds). (*Inset*) Time trajectories of the averaged dynamics of PTEN-TMR (red) and $PH_{Akt/PKB}$-EGFP (green).

Table S1. Model parameters

	Parameters	Values	Ref.
V_{PTEN}	Dephosphorylation rate of PtdIns(3,4,5)P_3 by PTEN	15 s^{-1}	(1)
K_{PTEN}	Michaelis constant of PTEN dephosphorylation reaction	50 molecules·μm^{-2}	(1, 2)
V_{PI3K}	Maximum velocity of PtdIns(4,5)P_2 phosphorylation by PI3K	600 molecules·μm^{-2}·s^{-1}	Assumed
K_{PI3K}	Michaelis constant of PI3K phosphorylation reaction	3500 molecules·μm^{-2}	(3)
λ_{PIP3}	PTEN-independent PtdIns(3,4,5)P_3 degradation rate	0.2 s^{-1}	Assumed
λ_{PIP2}	PI3K-independent PtdIns(4,5)P_2 degradation rate	0.002 s^{-1}	Assumed
D	Diffusion coefficient of PtdIns lipids on membrane	0.2 μm^2·s^{-1}	(4)
k	PTEN-independent PtdIns(4,5)P_2 supply rate	45 (35) molecules·μm^{-2}·s^{-1}*	(5)
V_{ass}	Association rate of PTEN to membrane	1300 molecules·μm^{-2}·μM^{-1}·s^{-1}	Assumed
K_{PIP2}	Michaelis constant of PtdIns(4,5)P_2 for PTEN association to membrane	3500 molecule·μm^{-2}	Assumed
λ_{PTEN}	Dissociation rate of PTEN from membrane	1.0 s^{-1}	(6)
K_α	†	120 molecules·μm^{-2}	Assumed
α	†	0.001	Assumed
K_β	‡	(100)	Assumed
β	‡	1 (0.8)	Assumed
$[PTEN]_{total}$	Total concentration of PTEN	0.1 μM	Typical
χ	A constant to transform surface concentration to volume concentration	10^{-3} μM·μm^2·molecules	Assumed
R	Cell radius	5 μm	Typical

*Without the PTEN-independent supply, the amount of PtdIns(3,4,5)P_3 and PtdIns(4,5)P_2 are exhausted due to the degradation of PtdIns(4,5)P_2. For the results shown in Fig. 5 *B–F* and *G Left*, the parameter value of supply rate is k = 45. For the results in Fig. 5*G Right*, k = 35.

†K_α is the half-maximum concentration of [PIP3] for PTEN association or dissociation from the membrane with $0 \leq \alpha \leq 1$. The values were inferred to satisfy the conditions that the number of PIP2 should be ~4000 molecules/μm^2 (7) and the period of oscillation should be 200 s.

‡K_β is the half-maximum concentration of [PIP3] for positive PI3K activation by PIP3 with $0 \leq \beta \leq 1$. For the results shown in Fig. 5 *C* and *F*, the parameter values of K_β and β are 100 and 0.8, respectively.

1. McConnachie G, Pass I, Walker SM, Downes CP (2003) Interfacial kinetic analysis of the tumour suppressor phosphatase, PTEN: evidence for activation by anionic phospholipids. *Biochem J* 371:947–955.
2. Gamba A, et al. (2005) Diffusion-limited phase separation in eukaryotic chemotaxis. *Proc Natl Acad Sci USA* 102:16927–16932.
3. Carpenter CL, et al. (1990) Purification and characterization of phosphoinositide 3-kinase from rat liver. *J Biol Chem* 265:19704–19711.
4. Fujiwara T, et al. (2002) Phospholipids undergo hop diffusion in compartmentalized cell membrane. *J Cell Biol* 157:1071–1081.
5. Zhang X, et al. (1997) Phosphatidylinositol-4-phosphate 5-kinase isozymes catalyze the synthesis of 3-phosphate-containing phosphatidylinositol signaling molecules. *J Biol Chem* 272: 17756–17761.
6. Vazquez F, et al. (2006) Tumor suppressor PTEN acts through dynamic interaction with the plasma membrane. *Proc Natl Acad Sci USA* 103:3633–3638.
7. Xu C, Watras J, Loew LM (2003) Kinetic analysis of receptor-activated phosphoinositide turnover. *J Cell Biol* 161:779–791

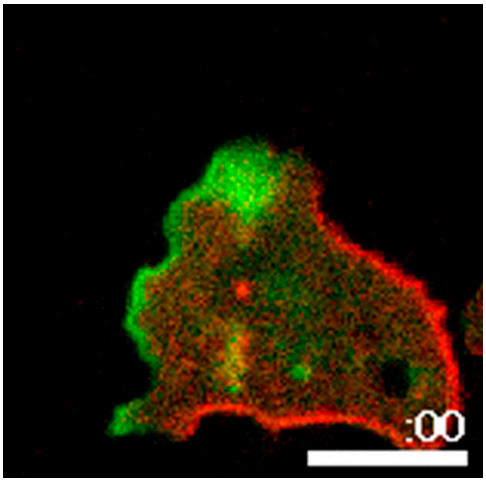

Movie S1. Simultaneous imaging of PTEN-TMR and $PH_{Akt/PKB}$-EGFP in locomoting *Dictyostelium* cells. $PH_{Akt/PKB}$-EGFP (green) was localized at the pseudopod regions, whereas PTEN-TMR (red) was localized at the lateral and tail regions of the cells. Time-lapse movies were acquired at 1-s intervals by using a confocal microscope. (Scale bar, 10 μm.) Time, :s (QuickTime; 384 KB).

Movie S1

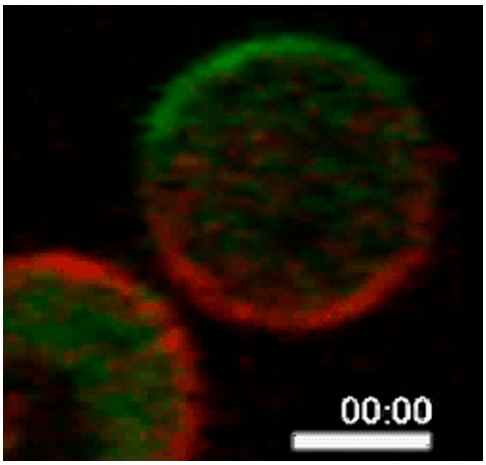

Movie S2. Simultaneous imaging of PTEN-TMR and $PH_{Akt/PKB}$-EGFP in *Dictyostelium* cells treated with 5 μM latrunculin A. PTEN-TMR (red) and $PH_{Akt/PKB}$-EGFP (green) were localized on the membrane, showing rotational traveling waves in a reciprocal manner. Time-lapse movies were acquired at 5-s intervals by using a confocal microscope. (Scale bar, 5 μm.) Time, min:s (QuickTime; 2.9 MB).

Movie S2

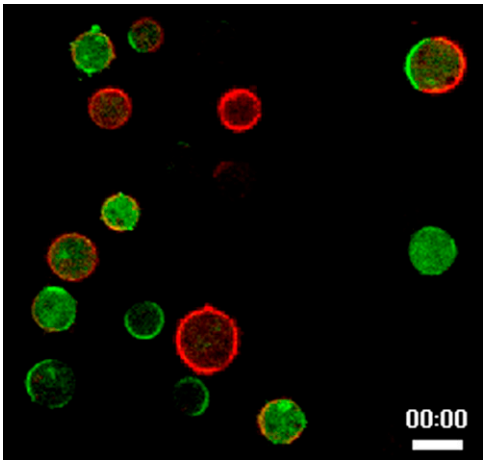

Movie S3. Simultaneous imaging of PTEN-TMR and $PH_{Akt/PKB}$-EGFP in *Dictyostelium* cells treated with 5 μM latrunculin A (same experimental condition as Movie S2). Most cells show reciprocal rotational traveling waves for PTEN-TMR (red) and $PH_{Akt/PKB}$-EGFP (green). Time-lapse movies were acquired at 5-s intervals by using a confocal microscope. (Scale bar, 10 μm.) Time, min:s (QuickTime; 3.6 MB).

Movie S3

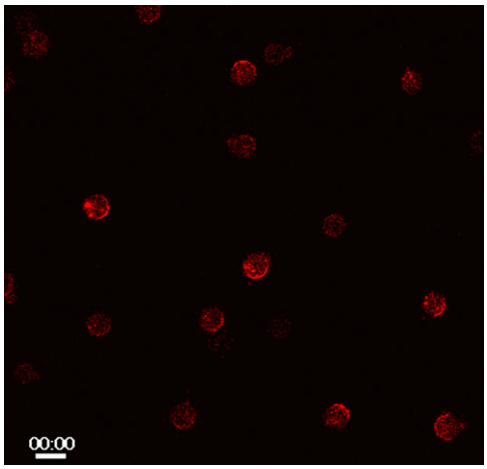

Movie S4. PTEN-TMR in *Dictyostelium* cells lacking functional *pi3k* genes (*pi3k1-5*$^{-}$, HM1200) treated with 5 μM latrunculin A. PTEN-TMR (red) showed polarized membrane localization without efficient rotation along the membrane in most cells. Time-lapse movies were acquired at 5-s intervals by using a confocal microscope. (Scale bar, 10 μm.) Time, min:s (QuickTime; 2.7 MB).

Movie S4

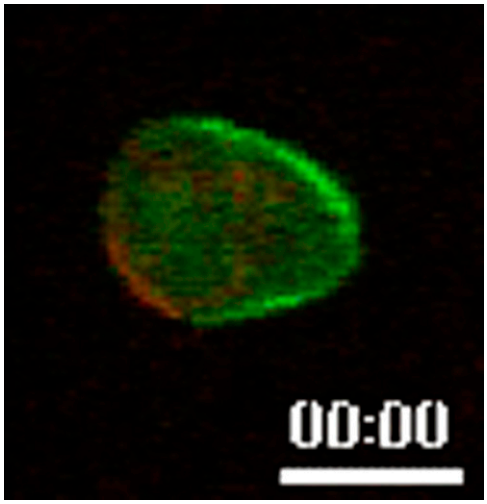

Movie S5. Simultaneous imaging of PTEN-TMR and $PH_{Akt/PKB}$-EGFP in *Dictyostelium* cells treated with 2.5 μM latrunculin A. The cells exhibited oscillatory behaviors. Time-lapse movies were acquired at 5-s intervals. (Scale bar, 10 μm.) Time, min:s (QuickTime; 1.3 MB).

Movie S5

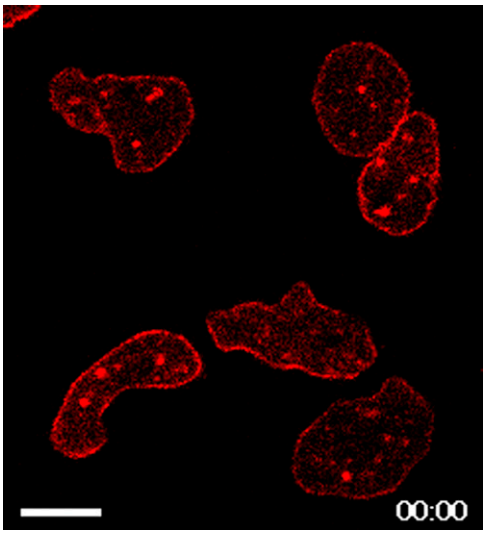

Movie S6. PTEN-TMR localization in locomoting *Dictyostelium pi3k1-5*-null cells. Cells often exhibit locomotion in one direction with continuous localization of PTEN-TMR (red) at the leading edge. In some cases, PTEN-TMR is excluded transiently from the leading edge. Cells were observed using an agar sheet as described in *SI Materials and Methods*. Time-lapse movies were acquired at 2-s intervals by using a confocal microscope. (Scale bar, 10 μm.) Time, min:s (QuickTime; 1.5 MB).

Movie S6

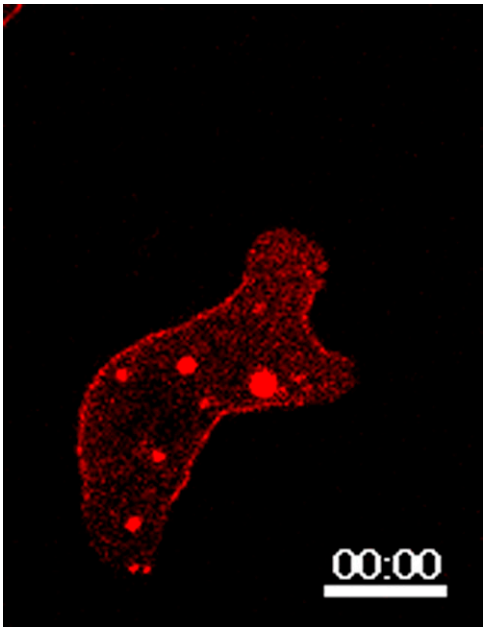

Movie S7. PTEN-TMR localization in locomoting *Dictyostelium* wild-type cells. PTEN-TMR (red) is excluded continuously from the leading edge pseudopod of the locomoting cell, which is consistent with previous observations (1, 2). Cells were observed at the same condition as described in Movie S6. (Scale bar, 10 μm.) Time, min:s (QuickTime; 2.0 MB).

Movie S7

1. Funamoto S, Meili R, Lee S, Parry L, Firtel RA (2002) Spatial and temporal regulation of 3-phosphoinositides by PI 3-kinase and PTEN mediates chemotaxis. *Cell* 109:611–623.
2. Iijima M, Devreotes P (2002) Tumor suppressor PTEN mediates sensing of chemoattractant gradients. *Cell* 109:599–610.